Transition state dynamics of OHF on several electronic states: Photodetachment spectrum of OHF^- and conical intersections

Lola González-Sánchez
Unidad Asociada UAM-CSIC, Instituto de Matemáticas y Física Fundamental, C.S.I.C., Serrano 123, 28006 Madrid, Spain and Departamento de Química Física, Facultad de Química, Universidad de Salamanca, 37008 Salamanca, Spain

Susana Gómez-Carrasco
Departamento de Química Física, Facultad de Química, Universidad de Salamanca, 37008 Salamanca, Spain and Unidad Asociada UAM-CSIC, Departamento de Química Física, Facultad de Ciencias C-XIV, Universidad Autónoma de Madrid, 28049 Madrid, Spain

Alfredo Aguado and Miguel Paniagua
Unidad Asociada UAM-CSIC, Departamento de Química Física, Facultad de Ciencias C-XIV, Universidad Autónoma de Madrid, 28049 Madrid, Spain

M. Luz Hernández
Departamento de Física de la Atmósfera, Facultad de Ciencias, Universidad de Salamanca, 37008 Salamanca, Spain

José M. Alvariño
Departamento de Química Física, Facultad de Química, Universidad de Salamanca, 37008 Salamanca, Spain

Octavio Roncero
Unidad Asociada UAM-CSIC, Instituto de Matemáticas y Física Fundamental, C.S.I.C., Serrano 123, 28006 Madrid, Spain

(Received 14 June 2004; accepted 25 August 2004)

Wave packet simulations of the photodetachment spectrum of OHF^- are performed on several electronic adiabatic states, two triplets and four singlets of neutral OHF. The transition moments to these six states have been approximated using the *ab initio* electronic wave functions of OHF^- and OHF calculated at the equilibrium configuration of the parent anion. In a first step, two-dimensional simulations of the spectrum are performed on new two-dimensional potential energy surfaces (PESs) of the neutral in a OHF collinear geometry. The resulting simulated spectrum is in rather good agreement with the experimental one, reproducing all the structures from 0 to 2.5 eV electron kinetic energies. At energies below 0.5 eV, all calculated states, singlets and triplets, contribute to the total spectrum. At higher energies, however, only the triplet states participate. In a second step, to improve the description of the spectrum, three-dimensional wave packet simulations of the spectrum are performed, getting an excellent agreement with the experiment. The collinear $^3\Sigma^-$ and $^3\Pi$ states split in two $^3A''$ and one $^3A'$. New adiabatic PESs are used in this work for the $2\,^3A''$ and $1\,^3A'$ states, while the one recently proposed was used for the ground $1\,^3A''$. It is found that the minimum energy paths of the $^3\Sigma^-$ and $^3\Pi$ states cross twice at collinear geometry, so that at the transition state the ground state corresponds to $^3\Pi$, while $^3\Sigma^-$ is the lowest state otherwise. Such conical intersections are expected to give rise to important Σ-Π vibronic effects, requiring a complete three-dimensional model of coupled diabatic states to improve our understanding of the reaction dynamics in this kind of systems. © *2004 American Institute of Physics.*
[DOI: 10.1063/1.1807375]

I. INTRODUCTION

There is great interest to study the dynamics of the O + H*X* (*X*=halogen atom) reactions because of their contribution to the catalytic ozone destruction cycle.[1] Among them, O+HCl has been the most widely studied[2–16] but OHF constitutes a convenient benchmark because its relative simplicity makes easier the calculation of the many electronic states involved. Recently, we have studied the reactive OH+F collision[17,18] on a new three-dimensional potential energy surface of the $1\,^3A''$ electronic state. The final vibrational distributions of HF products and rate constants obtained[17] were in rather good agreement with the available experimental data.[19,20]

It was found[18] that below the kinetic threshold (due to the bending zero-point energy at the transition state region), the reaction is mediated by resonances. These resonances are found not only in wave packet simulations but also in quasiclassical trajectories as a manifestation of pretty stable periodic orbits. Above this threshold the reaction dynamics is direct. Such resonances also appear in the theoretical simu-

lations of the photodetachment spectrum and in Ref. 21 they were interpreted as heavy-light-heavy-type resonances due to the van der Waals wells in the two rearrangement channels of the $1\,^3A''$ state. Some of these resonances are grouped in regions where the experimental spectrum[22] shows bands. However, this assignment seemed to be doubtful. In addition, in previous two-dimensional simulations of the photodetachment spectrum,[22,23] these resonances do not appear.

The two rearrangement asymptotes, F+OH and O+HF, correspond to open shell systems, in which there are several degenerate states. In the $F(^2P)+OH(^2\Pi)$ dissociative limit there are 24 electronic potential energy surfaces (PESs). The first three triplets, triply degenerate, correlate with $O(^3P)+HF(^1\Sigma^+)$. There are also some other singlet states which correlate with the $O(^1D)+HF(^1\Sigma^+)$ asymptote. All of them may contribute to the photodetachment spectrum, but until now only the ground triplet and the first singlet states have been taken into account.[22,23]

The purpose of this work is to determine the contribution of each of the electronic states associated to the $OH(^2\Pi)+F(^2P)$ asymptote, without considering spin-orbit effects. The spin-orbit splittings of $F(^2P)$, $O(^3P)$, and $OH(^2\Pi)$ are 50, 28, and 15 meV, respectively, small as compared with the larger separation between the experimental bands in the experimental photodetachment experiment,[22] of the order of 0.5 eV. The inclusion of spin-orbit terms would split the states involved in quantities of this order, $\approx$50 meV, leading to an additional average in the spectrum which would tend to wash out the bands of the spectrum. The transitions among spin-orbit sublevels could add some interesting features to the reaction dynamics at the transition state, but the photodetachment spectrum, at least for the experimental resolution now a days available,[22] would remain essentially the same. For this reason, the neglect of spin-orbit effects is considered to be rather good. For reactive collisions, however, such effects could have a larger effect, as, for example, in affecting the partition function among different sublevels.

The transition dipole moments are modelized using the calculated electronic wave functions of the OHF^- anion at the equilibrium geometry. The spectrum is then simulated, first, using two-dimensional PESs for the first six electronic states, reaching a rather good agreement with the experimental data of Bradforth *et al.*[22] Second, the spectrum is simulated for the first three triplet states using new three-dimensional surfaces, getting an even better agreement with the experiment. For the $1\,^3A''$ state we take the spectrum already calculated in Ref. 21 in a recent PES,[18] while for the $2\,^3A''$ and $1\,^3A'$ states new PESs are used. Finally, the conical intersections between these states are described and the role of Σ-Π vibronic effect is discussed.

II. METHOD FOR PHOTODETACHMENT PROCESS CALCULATION

The photodetachment processes of the OHF^- anion,

$$OHF^-(^2\Pi)+h\nu \rightarrow O(^3P,^1D)+HF(^1\Sigma^+)+e \rightarrow F(^2P)+OH(^2\Pi)+e,$$

are rather complicated to be simulated exactly because they involve the fragmentation in three fragments in different rearrangement and electronic channels. The most common approximation[24–26] relies on the time scale difference between the detached electron dynamics and the subsequent reaction dynamics of the neutral fragments: since the electron departs very rapidly as an *s* wave, it is assumed that it does not strongly affect the neutral subsystem. The conservation of the total energy imposes $\epsilon = h\nu + E_{OHF^-} - E$, where ϵ is the electron kinetic energy, E is the total energy of the OHF neutral fragments, and E_{OHF^-} is the energy of the parent anion state. Because all dependence on the kinetic energy of the departing electron will be neglected, ϵ becomes an external parameter depending on the energy of the incident photon and the total neutral energy. Thus, the photodetachment spectrum as a function of the electron kinetic energy can be alternatively expressed in terms of the energy of the neutral.

Furthermore, assuming a first-order perturbative treatment for electric dipole transitions between an initial electronic state of the anion, χ_α^-, and a final electronic state of the neutral, $\chi_{\alpha',\epsilon}$, the spectrum can be obtained in a wave packet treatment as

$$\sigma_{k\alpha,\alpha'}(E) = \frac{1}{\pi\hbar}\mathcal{R}\int_0^\infty dt e^{iEt/\hbar}\langle \Psi_{\alpha k}^{JMp\alpha'}(t=0)|\Psi_{\alpha k}^{JMp\alpha'}(t)\rangle, \tag{1}$$

where $\Psi_{\alpha k}^{JMp\alpha'}(t)$ is the nuclear part of the wave packet, expanded as

$$\Psi_{\alpha k}^{JMp\alpha'}(\mathbf{r},\mathbf{R},t) = \sum_\Omega \mathcal{W}_{M\Omega}^{Jp}(\phi,\theta,\chi)\Phi_{\alpha k\Omega}^{Jp\alpha'\Omega}(r,R,\gamma,t), \tag{2}$$

where $\Phi_{\alpha k\Omega}^{Jp\alpha'\Omega}(r,R,\gamma,t)$ are coefficients depending on the internal coordinates which are obtained by numerically integrating the time dependent Schrödinger equation using the PES of the α' final electronic state of OHF. $\mathcal{W}_{M\Omega}^{Jp}$ are linear combinations of Wigner rotation matrices with well defined parity under inversion of spatial coordinates, *p*, for a total nuclear angular momentum *J*. *M* and Ω are the projections of the total angular momentum in the space-fixed and body-fixed *z* axes, respectively, which are related by a rotation parametrized by (ϕ,θ,χ) Euler angles. Such angles are defined by the election of the body-fixed frame. In the present case two sets of Jacobi coordinates are used, for reactants and products, but in the two cases the three atoms lie in the *x*-*z* plane. The two Jacobi vectors are **r**, the *A*H internuclear vector, and **R**, which joins the *A*H center of mass to the *B* atom, with γ being the angle between them. The *z* axis is defined parallel to **R**. *A*H corresponds to OH or HF molecules for reactant and product Jacobi coordinates, respectively.

Assuming that the ejected electron departs with zero orbital momentum, the electronic orbital angular momentum does not change in the photodetachment process. The electron does only carry spin angular momentum, thus allowing transitions between doublet states of OHF^- towards both

singlet and triplet states of the neutral OHF. In this regard, for final triplet states there are four possible transitions among spin projections, $1\leftarrow 1/2$, $-1\leftarrow -1/2$, and $0\leftarrow \pm 1/2$, while for singlet states only the last two transitions are possible. Because of this, the absorption intensity is multiplied by $N_{\alpha'}=2(S+1)$, S being the electronic spin of the final electronic state.

Using an adiabatic approximation, the initial wave packet is defined to describe a given $J'\leftarrow J$ rotational electric dipole transition as[27,28]

$$\Psi_{\alpha k}^{JMp\alpha'}(t=0)=\sum_{\Omega'}\mathcal{W}_{M'\Omega'}^{J'p'}\langle\mathcal{W}_{M'\Omega'}^{J'p'}|\mathbf{d}^{\alpha'\epsilon,\alpha}\cdot\mathbf{e}|\varphi_k^{JMp\alpha}\rangle, \tag{3}$$

where $\varphi_k^{JMp\alpha}$ corresponds to the k vibrational state of the OHF^- anion in the α electronic state. The ground electronic states of OHF^- are $^2\Pi$ in collinear geometry, which split in $^2A'$ and $^2A''$ states as the system bends as shown previously.[21] However, in the present treatment, Renner-Teller effects are neglected and the two states are considered to be uncoupled and degenerate.

In Eq. (3), **e** is the polarization vector of the incident photon while $\mathbf{d}^{\alpha'\epsilon,\alpha}$ is the electric dipole transition moment between the initial electronic state of OHF^-, χ_α^-, and the final electronic wave function of OHF times the departing electron. These matrix elements are considered to be independent of the nuclear degrees of freedom in the localized region of the initial vibrational state of the anion, and independent of the kinetic energy of the departing electron. With this restriction being applied to a linear equilibrium configuration, the electric dipole moment can be approximated by

$$\mathbf{d}^{\alpha'\epsilon,\alpha}(r,R,\gamma)\approx d^{\alpha',\alpha}(r_e,R_e,\gamma_e)\mathbf{u}_d,$$

as a multiplicative constant plus a geometric factor, where $\mathbf{u}_d$ is a unit vector which coincides with the molecular z axis in parallel transitions ($\Lambda_{\alpha'}=\Lambda_\alpha$) or with x, y axes in perpendicular transitions ($\Lambda_{\alpha'}=\Lambda_\alpha\pm 1$), where Λ_α is the projection of the electronic orbital angular momentum on the z axis.

With all these approximations, the total photodetachment cross section for producing electrons at energy ϵ is obtained as

$$\sigma(\epsilon=h\nu+E_{OHF}^--E)$$

$$=\sum_k\sum_\alpha\sum_{\alpha'}N_{\alpha'}|d^{\alpha',\alpha}(r_e,R_e,\gamma_e)|^2\sigma_{k\alpha,\alpha'}^0(E), \tag{4}$$

where $\sigma_{k\alpha,\alpha'}^0(E)$ is given in Eq. (1) but with a initial wave packet in Eq. (3) where the numerical $d^{\alpha',\alpha}(r_e,R_e,\gamma_e)$ factor is removed, leaving the geometry factors introduced through the Clebsch-Gordan coefficients.

III. ELECTRIC DIPOLE TRANSITION MOMENTS

The equilibrium configuration of the anion corresponds to a linear geometry with $r_{OH}=1.08$ Å and $r_{FH}=1.30$ Å with the hydrogen between the two heavier atoms.[21] At this geometry a complete active space self-consistent field (CASSCF) calculation on the OHF^- system is performed to obtain the molecular orbitals. These orbitals are used to build the wave functions of OHF^- and OHF, which are of crucial importance in the treatment that follows, and are shown in Fig. 1. The first four σ orbitals correspond essentially to linear combinations of the $1s$ and $2s$ atomic orbitals of F and O. $5\sigma/6\sigma$ orbitals are bonding/antibonding molecular orbitals in which the $2p_z$ of F and O and $1s$ of H atomic orbitals of the three atoms participate. Finally, $1\pi_x/2\pi_x$ bonding/antibonding orbitals are localized essentially on the F/O atoms.

The electronic wave functions are obtained for OHF^- and OHF using a multireference configuration interaction (MRCI) method,[29] and they are linear combinations of the form

$$\chi_\beta=\sum_i C_i^\beta\mathcal{D}_i, \tag{5}$$

where each configuration is represented by a Slater determinant $\mathcal{D}_i$ expressed in terms of the same set of molecular orbitals for OHF^- as for OHF. All the calculations were performed using the MOLPRO package.[29] It turns out that the two degenerate $^2\Pi$ states of OHF^- correspond to nearly one single configuration, either

$$\chi_{^2\Pi_x}^-=|1\sigma^2 2\sigma^2 3\sigma^2 4\sigma^2 5\sigma^2 1\pi_x^2 1\pi_y^2 6\sigma^2 2\pi_x^1 2\pi_y^2| \tag{6a}$$

or

$$\chi_{^2\Pi_y}^-=|1\sigma^2 2\sigma^2 3\sigma^2 4\sigma^2 5\sigma^2 1\pi_x^2 1\pi_y^2 6\sigma^2 2\pi_x^2 2\pi_y^1|, \tag{6b}$$

in very good agreement with previous results.[22]

In contrast, the electronic wave functions of the different states of OHF usually include several configurations. Now, the problem is to build a wave function corresponding to OHF plus one electron in the continuum $(OHF+1e)$. Such wave functions are approximated by including a singly occupied dissociative orbital σ_d in each configuration, as it is shown in Table I. Thus the configurations of the $(OHF+1e)$ joint system can be viewed as monoexcitation biexcitations, etc., of the reference configurations describing $OHF^-(^2\Pi)$. In a crude approximation, it can be considered that an electron is detached by promoting it from an occupied orbital of the OHF^- state, let us call it λ^0, towards the dissociative σ_d orbital, leaving the rest of the electrons in the same orbital they were. Such direct excitations would lead to monoexcited configurations of $(OHF+e)$, with $n_{ex}=1$. After the first electron departs, the rest of electrons quickly reorder among different configurations, yielding to the electronic states of the neutral OHF in which more configurations appear as can be seen in Table I. Such reordering would change a second electron from one of the orbitals of the OHF core. Thus, these configurations would correspond to higher order excitations, i.e., $n_{ex}\geqslant 2$, with respect to the reference configurations of OHF^- in Eq. (6).

The electric dipole operator is monoelectronic and its matrix elements between configurations differing in more than one molecular orbital, which must be orthonormal, are zero.[30] In the wave function of $(OHF+e)$, those configurations j corresponding to monoexcitations, $n_{ex}^{j,i}=1$ (with re-

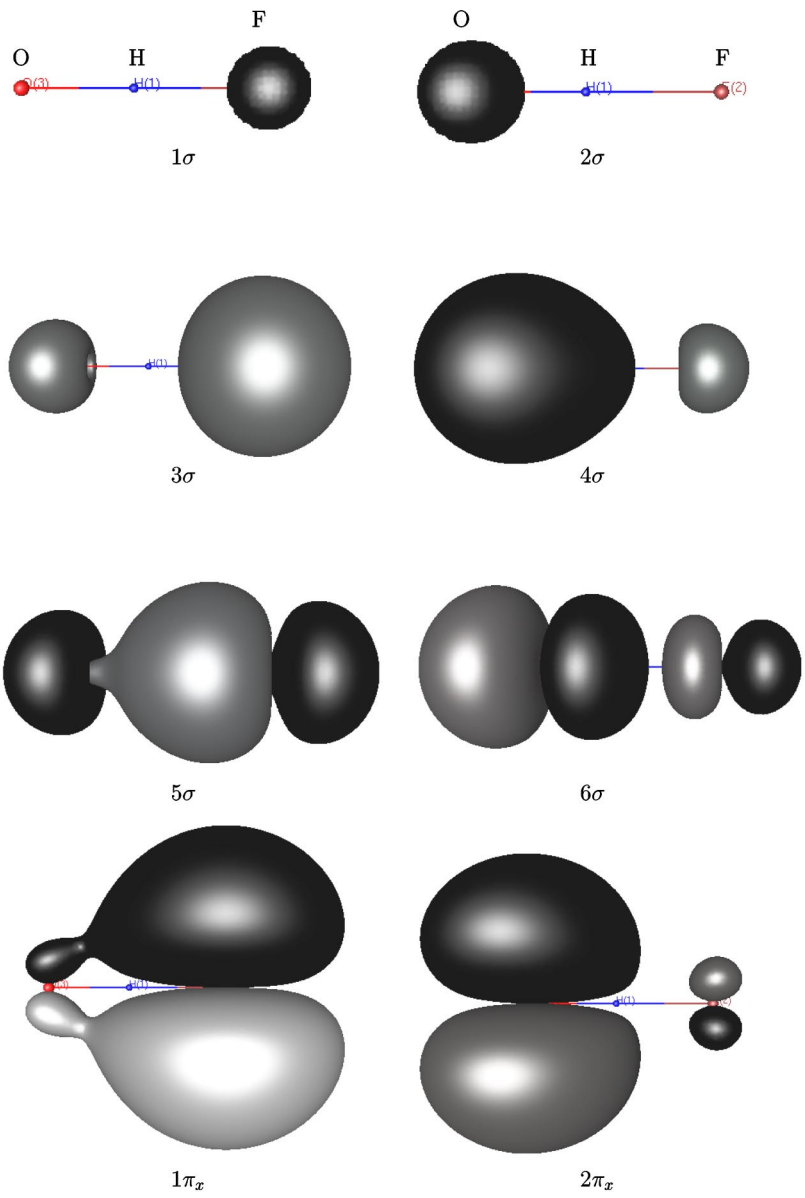

FIG. 1. Molecular orbitals obtained with the CASSCF method for OHF^-, and used for the MRCI wave functions of both OHF and OHF^- systems to evaluate the transition matrix elements. They correspond to collinear OHF nuclear configuration.

spect to configuration i of the anion wave function), do contribute to the electric dipole matrix element, because they are "bright" configurations directly reached in the photon excitation. However, those $(OHF+e)$ configurations with $n_{ex}^{j,i} \geqslant 2$ do not contribute to the electric dipole matrix element, because they are not directly excited, but reached through a "dark" reordering mechanism. An example is shown in Table I. When $n_{ex}^{j,i}=1$, the electric dipole matrix elements between the initial and final configurations reduce to the integral between the dissociative orbital σ_d and the orbital where the detached electron was in OHF^-, λ_j^0. Thus the electric dipole matrix elements become

$$d^{\alpha',\alpha}=\sum_j \sum_i \delta_{n_{ex}^{j,i},1} C_j^{\alpha'}(\mathrm{OHF}) C_i^{\alpha}(\mathrm{OHF}^-)\langle \sigma_d|\mathbf{q}|\lambda_j^0\rangle, \tag{7}$$

where $\mathbf{q}$ is the position vector of an electron. Now, assuming that σ_d is nearly constant in the molecular region because it corresponds to low electron kinetic energy, $\langle \sigma_d|\mathbf{q}|\lambda_j^0\rangle$ can be considered to be nearly independent of the particular λ_j^0 orbital. Then, with this simple approximation, the electric dipole moments can be approximated by

$$d^{\alpha',\alpha} \propto \sum_j \sum_i \delta_{n_{ex}^{j,i},1} C_j^{\alpha'}(\mathrm{OHF}) C_i^{\alpha}(\mathrm{OHF}^-). \tag{8}$$

Thus, the allowed transitions are from the $OHF^-(\Pi_{x,y})$ states towards the $OHF(\Sigma^+,\Sigma^-,\Pi_{x,y},\Delta_{x,y})$ states, and the numerical values are shown in Table I. It is seen that the $\Pi \leftarrow \Pi$ excitations mainly correspond to the promotion of one electron from a σ orbital, while $\Delta, \Sigma \leftarrow \Pi$ transitions typically involve the promotion from π orbitals.

In the anion, the charge in excess is distributed among the O and F atoms, leaving the hydrogen atom nearly neutral (with a small positive effective charge) in the middle. Such result is obtained from a Mulliken charge density analysis and it can be illustrated by plotting the electronic density difference of the OHF^- anion, obtained by subtraction of the electronic density of isolated neutral atoms from that of the

TABLE I. Electronic states of the (OHF+e) system, α', expressed in terms of the dominant configurations, with a coefficient larger than 0.1. The excitation order of the configurations with respect to the $^2\Pi_x$ and $^2\Pi_y$ states of the OHF^- anion are also given. Finally, the corresponding transition dipole moment, $d^{\alpha',\alpha}$, is shown in the last column, calculated according to the method explained in the text.

α'	$\lvert 5\sigma 1\pi_x 1\pi_y 6\sigma 2\pi_x 2\pi_y \sigma_d \rvert$							$C_j^{\alpha'}$	$n_{ex}(^2\Pi_x)$	$n_{ex}(^2\Pi_y)$	$d^{\alpha',^2\Pi_x}$	$d^{\alpha',^2\Pi_y}$
$^3\Sigma^-$	2	1	2	2	2	1	1	$\approx -1/\sqrt{2}$	2	1	$1/\sqrt{2}$	$-1/\sqrt{2}$
	2	2	1	2	1	2	1	$\approx 1/\sqrt{2}$	1	2		
$^3\Pi_x$	2	2	2	1	1	2	1	0.95	1	2	≈ 1	0
$^3\Pi_y$	2	2	2	1	2	1	1	0.95	2	1	0	≈ 1
$^1\Pi_x$	2	2	2	1	1	2	1	0.95	1	2	≈ 1	0
$^1\Pi_y$	2	2	2	1	2	1	1	0.95	2	1	0	≈ 1
$^1\Delta_x$	2	2	1	2	2	1	1	$\approx 1/\sqrt{2}$	2	1	$1/\sqrt{2}$	$1/\sqrt{2}$
	2	1	2	2	1	2	1	$\approx 1/\sqrt{2}$	1	2		
$^1\Delta_y$	2	1	2	2	2	1	1	$\approx -1/\sqrt{2}$	2	1	$1/\sqrt{2}$	$-1/\sqrt{2}$
	2	2	1	2	1	2	1	$\approx 1/\sqrt{2}$	1	2		
$^1\Sigma^-$	2	2	2	2	1	1	1	-0.29	1	1	≈ 0.35	≈ 0.35
	2	1	2	2	2	1	1	0.64	2	1		
	2	2	1	2	1	2	1	0.64	1	2		
	2	1	1	2	2	2	1	-0.18	2	2		
$^1\Sigma^+$	2	2	1	2	2	1	1	0.64	2	1	≈ 0.5	≈ 0.5
	2	1	2	2	1	2	1	-0.64	1	2		
	2	2	2	2	0	2	1	0.18	1	2		
	2	2	2	2	2	0	1	-0.18	2	1		

OHF^- anion, as shown in Fig. 2. This figure has to be taken as merely informative, since it depends on the electronic state of neutral atom being chosen in a open $O(^3P)$ or $F(^2P)$ shell. This has been done to obtain density differences with a proper symmetry with respect to the x-z plane. Comparing this density difference to the shapes of the promoted nuclear orbitals, in Fig. 1, provides a simple picture of the nature of the electronic transition involved for each final electronic state of OHF.

IV. TWO-DIMENSIONAL SIMULATIONS

Aside from the electronic selection rules, the nuclear Frank-Condon factors will determine whether or not a given final electronic state contributes to the spectrum in a given energy interval. For this purpose, independent two-dimensional wave packet calculations were done for each individual final electronic state, all of them correlating with $OH(^2\Pi)+F(^2P)$. The zero of energy is referred to $OH(v=0)+F$. The triplets correlate with $O(^3P)+HF(^1\Sigma^+)$ product channel, which is at ≈ -1.5 eV. The singlets, however, correlate with $O(^1D)+HF(^1\Sigma^+)$ products which are at about 0.5 eV. The collinear minimum energy path between reactants and products is summarized in Fig. 3. Until now, only the $^3\Pi$ and $^1\Delta$ excited states had been computed[19] and

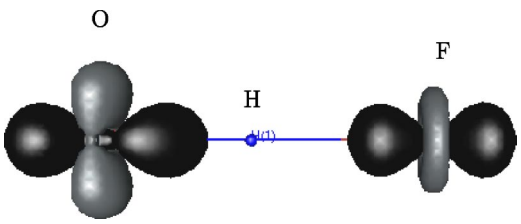

FIG. 2. Electronic density difference of OHF^- at its equilibrium configuration. The difference is obtained by subtracting the density associated to the free neutral atoms from that of the OHF^- anion.

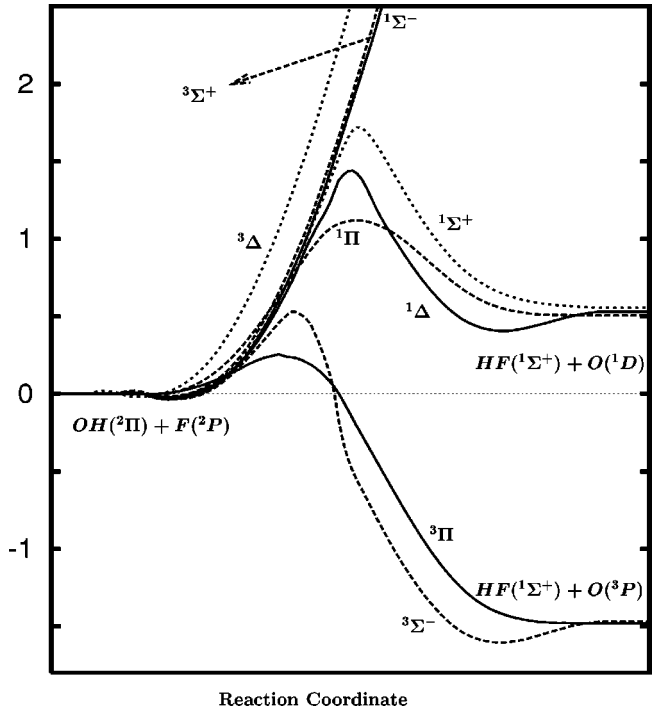

FIG. 3. Collinear minimum energy path (in eV) for several electronic states of OHF including asymptotic rearrangement channels.

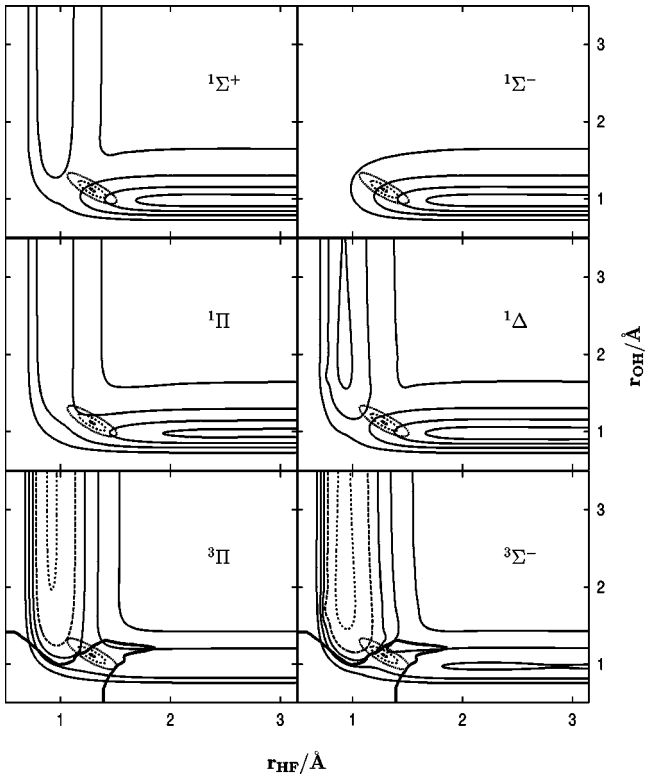

FIG. 4. Contour plots of the PES calculated for several electronic states of OHF at collinear configuration. Plotted are the four singlet and the two relevant triplet states (see also Fig. 3). The contours are −1.4, −0.6 (shown as dashed lines), 0, 0.8, and 2 eV for triplets and 0.1, 0.5, 1.3, and 3 eV for singlets. All energies are referred to the F+OH minimum at the asymptote. The initial wave packet is also shown in all panels, placed in the region of the transition state. In the bottom panels, the intersection seam between the $^3\Sigma^-$ and $^3\Pi$ states is shown as a thick line: inside/outside this line the $^3\Pi/^3\Sigma^-$ state has lower energy.

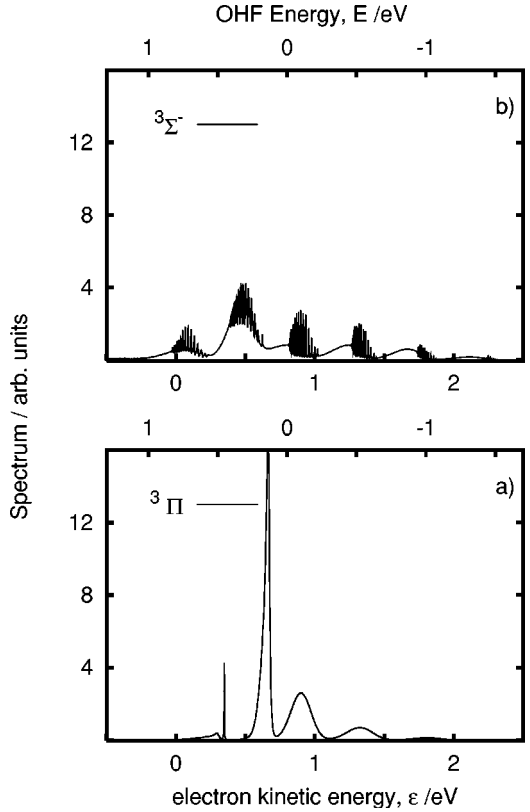

FIG. 5. Calculated photodetachment spectra for triplet electronic states of OHF in collinear configuration as a function of the electron kinetic energy (lower scale) and the internal OHF energy (upper scale) for (a) $^3\Pi$ and (b) $^3\Sigma^-$ states.

used in the photodetachment simulations,[22] but these PESs were not too accurate. Later on, Dixon and Tachikawa[23] improved the $^3\Pi$ PES at collinear configurations. Very recently, we have simulated the photodetachment spectrum on a three-dimensional PES (Ref. 21) of the $^3A''$ state.

The PES for two triplet states and four singlet states have been calculated at collinear configuration, and their contour plots are shown in Fig. 4. These PESs have been generated by bidimensional spline interpolation[31] of *ab initio* calculations in a grid of points for collinear OHF configurations defined as $1.1 \leqslant R_{OH} \leqslant 7.2$ and $1.3 \leqslant R_{HF} \leqslant 6a_0$, using 42 and 17 points, respectively, not equally spaced. Details of the *ab initio* calculations are discussed in Ref. 18. In this case, a C_{2v} point group has been used, which allows the clear identification of the symmetry of the electronic states.

The two-dimensional wave packet calculations are done in reactant Jacobi coordinates using the same three-dimensional calculations described elsewhere,[21] but assuming that the potential is isotropic, thus only including OH rotational functions with $j=0$. The wave packet is represented in a 256×512 bidimensional radial grid of equidistant points, in the intervals $0.4 \leqslant r \leqslant 9$ Å and $0.75 \leqslant R \leqslant 20$ Å, respectively. The time integration is performed up to 5–10 ps, using a Chebyshev propagator[32,33] with a time step of 0.25 fs. Such small time step is required to calculate the spectra which are distributed in a rather broad energy range. After each time step the wave packet is absorbed at the edges of the grid by multiplying it by a Gaussian damping function beyond $r_{abs}=6$ Å, and $R_{abs}=13$ Å. The exponential coefficients of the Gaussian functions were optimized to avoid reflections.

The three triplet states, two degenerate $^3\Pi$ and one $^3\Sigma^-$, correlating with the $O(^3P)+HF(^1\Sigma^+)$ asymptote, cross each other along the minimum energy path (MEP): $^3\Pi$ has lower energy at the saddle point, but the two wells, in the reactant and products channels, belong to the $^3\Sigma^-$ state. The seam crosses twice the collinear MEP before and after the saddle point approximately in a perpendicular way, and it is shown in the panel for $^3\Pi$ and $^3\Sigma^-$ of Fig. 4.

As shown in Fig. 5 the calculated spectra for the $^3\Pi$ and the $^3\Sigma^-$ states are quite different. In fact, the spectrum of the $^3\Pi$ state does not show any resonant structure and is formed by several broadbands, in pretty good agreement with that obtained by Dixon and Tachikawa.[23] The resonant structure is present in the spectrum obtained for the $^3\Sigma^-$ state, which supports the two wells. At the equilibrium OHF^- configuration, the vertical excitation to $^3\Pi$ is at much lower energy than that of $^3\Sigma^-$, by ≈0.3 eV. However, the initial wave packet overlaps significantly with the regions of the two wells of the $^3\Sigma^-$ state, due to the spreading of the ground vibrational state in OHF^-. These crossings will strongly affect the spectra obtained for the three-dimensional adiabatic surfaces, as will be discussed below.

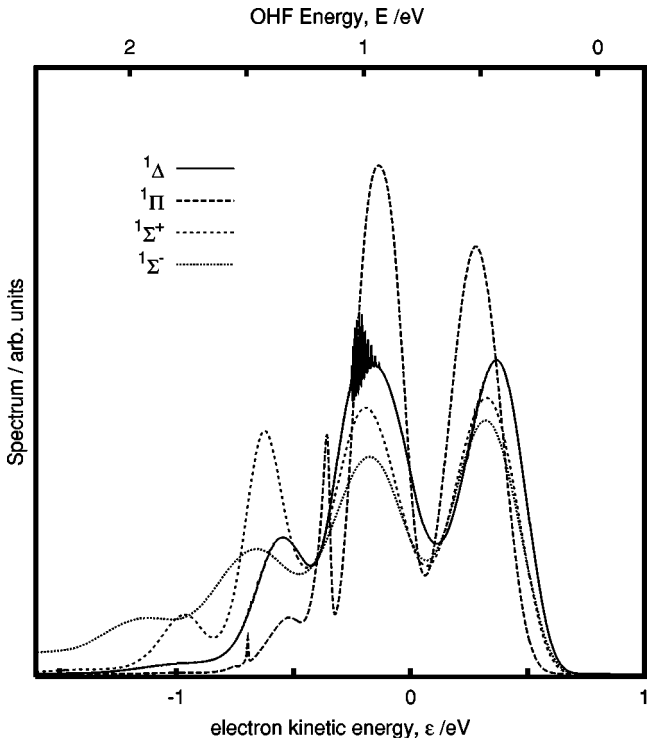

FIG. 6. Calculated photodetachment spectra for singlet electronic states of OHF in collinear configuration as a function of the electron kinetic energy (low scale) and the internal OHF energy (upper scale).

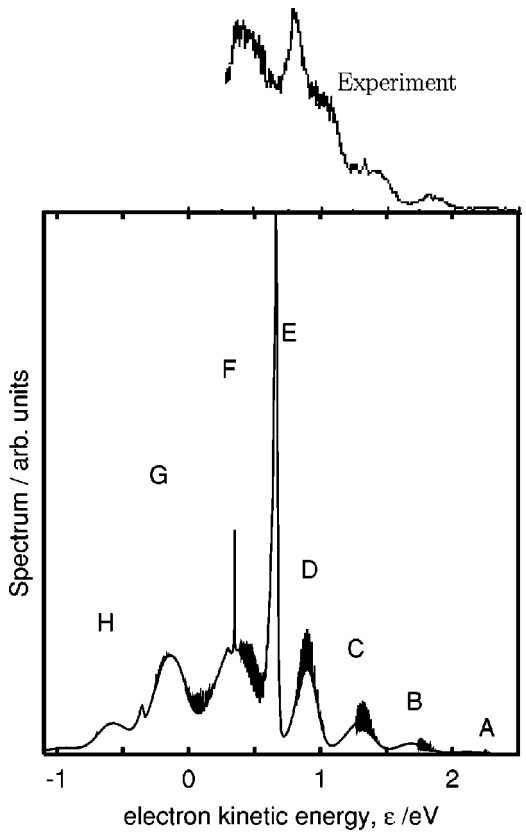

FIG. 7. Calculated photodetachment spectra obtained after averaging over all final electronic states according to the transition matrix elements and multiplicity, as explained in the text. The experimental spectrum of Bradforth *et al.* (Ref. 22) is also shown for comparison.

The four singlet states correlating with the $O(^1D)+HF$ asymptote, also absorb but at higher OHF energies as can be seen in Fig. 6. At lower energies $F+OH(^2\Pi)$ is the only open dissociation channel. It is only above 0.5 eV that the $O(^1D)+HF$ channel opens. The experimental peak at low kinetic energies, labeled by F,[22] is therefore attributed to all these singlet states and also to the $^3\Sigma^-$, to some extent. Unfortunately, at the experimental wavelength used, 213 nm, the whole spectrum of these states cannot be accessed. This is the reason why the theoretical simulations present amplitude at "negative kinetic energy." It would be interesting to increase the excitation energy of the incident photon to access these states. Alternatively, these states can be reached in photodissociation experiments from the deep well in the $^1A'$ state (minimum at FOH internal angle $\approx 60°$) as performed for OHCl.[34–36]

In order to compare with the experimental spectrum, the total spectrum averaging over all final electronic states, according to Eq. (4), is computed and shown in Fig. 7. The agreement with the experimental spectrum[22] is excellent, reproducing all the bands labeled from A to F in decreasing order with respect to the electron kinetic energy. Bands A to D correspond to HF vibrational states $v=0$, 1, 2, and 3, respectively, in the three $^3\Pi$ and $^3\Sigma^-$ electronic states. Band A is attributed to only $^3\Sigma^-$: no wonder that Dixon and Tachikawa[23] did not find it using only the $^3\Pi$ state. Band D is modified by the opening of the $OH(v=0)$, which is not too clearly seen in the two-dimensional model. Band E is due to a narrow peak of the $^3\Pi$. When compared to the experimental one, it is by far too narrow and too intense. However, when performing three-dimensional calculations these two structures are very much modified, becoming broader and less intense, in better agreement with the experiment, as will be discussed below. Peak F has contributions from all the electronic states and it is therefore difficult to assign. The new bands appearing, labeled here G and H, are due to singlet states and could be measured by using shorter wavelength excitation lasers.

V. THREE-DIMENSIONAL SIMULATIONS FOR TRIPLET STATES

As noted above, it is necessary to perform a three-dimensional model to better describe the photodetachment spectrum. In this work we focus on the triplet states joining the $OH(^2\Pi)+F(^2P)$ and $HF(^1\Sigma^+)+O(^3P)$ asymptotes, because they are the lower states which are responsible for the spectrum above 0.5 eV electron kinetic energies.

For the ground $1\,^3A''$ adiabatic state the photodetachment spectrum has been previously calculated and its features assigned[21] using a recently developed three-dimensional PES.[18] Here, this spectrum will be used for comparing the other two excited triplet states spectra, $2\,^3A''$ and $1\,^3A'$. Global PESs for these two last states have been recently proposed and will be presented elsewhere.[37] Here they are used to obtain their contribution to the photodetachment spectrum and will only be briefly described. Also, all

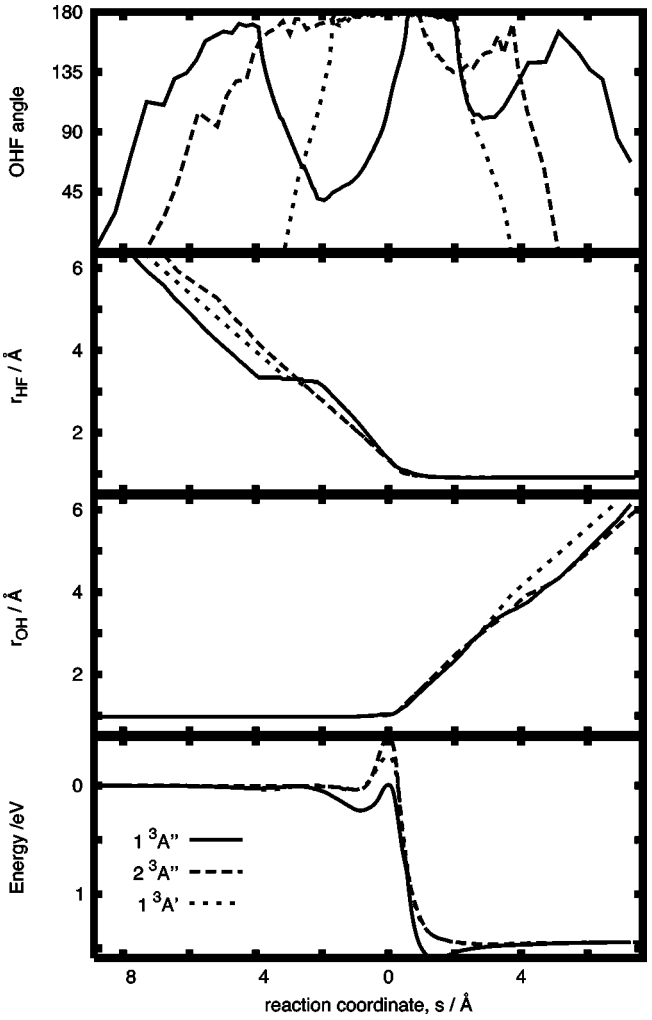

FIG. 8. Variation of the potential energy (i.e., minimum energy path or MEP) (bottom panel) and the internal coordinates (remaining panels) along the reaction coordinate for the three-dimensional PESs of the triplet adiabatic states of OHF.

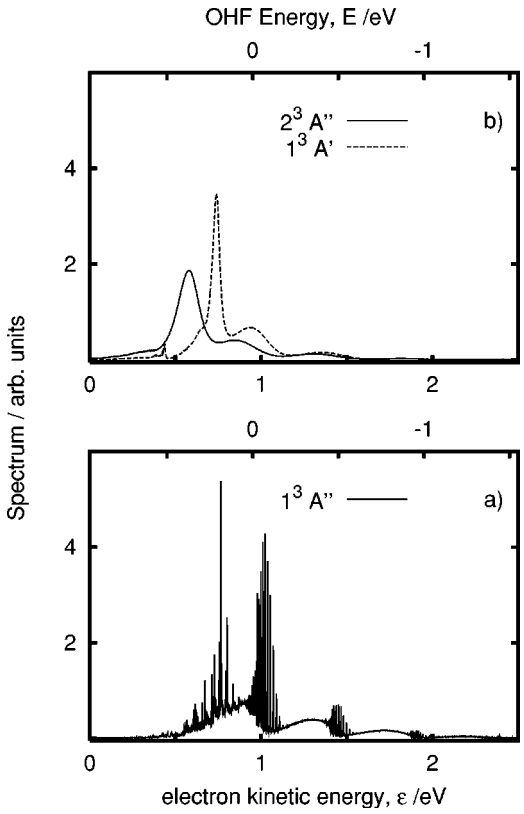

FIG. 9. Calculated photodetachment spectra for triplet electronic states of OHF using the fitted three-dimensional adiabatic surfaces as a function of the electron kinetic energy (lower scale) and the internal OHF energy (upper scale) for (a) $1\,^3A''$ and (b) $1\,^3A'$ and $2\,^3A''$ states.

the details of the wave packet calculations performed to obtain the spectra and their assignment have been presented in Ref. 21.

Some aspects of the topology of the 3D adiabatic PESs for the three triplet states are given in Fig. 8. The minimum energy paths are shown in the bottom panel and the variation along the reaction coordinate of the corresponding internal geometric parameters of the triatom in the other panels. The most important result is that while the adiabatic ground PES $1\,^3A''$ has a bent transition state this structure is linear for the excited triplet PES. The $1\,^3A''$ shows two wells, in the reactant and product channels, respectively. Also, it presents the lower saddle point, at bent geometries. These wells give rise to the appearance of many resonances in the corresponding photodetachment spectrum, in Fig. 9(a). Above the OH+F dissociation threshold, the resonances of the $1\,^3A''$ spectrum are of HLH character, with the light H atom oscillating between the two heavier atoms and exploring the transition state region, as deeply discussed in Ref. 21. The importance of these HLH resonances is that they, too, mediate the reaction in the OH+F collisions at low energies.[18]

The interest of these features of the $1\,^3A''$ spectrum is that, at collinear geometries, the wells correspond to the $^3\Sigma^-$ state while the saddle point correspond to the $^3\Pi$ state. That is, the HLH resonances and the reaction dynamics in general correspond to motions on two conical intersections whose seam is shown in Fig. 4. As the system bends the $^3\Sigma^-$ interacts with the $^3\Pi$ states through a Σ-Π vibronic mechanism[38] producing the three adiabatic states, with the ground one showing a well for bent configurations. Thus, the bent character of the saddle point of the $1\,^3A''$ is explained by this Σ^--Π vibronic effect. To illustrate these effects, in Fig. 10, the dependence of the PESs of the three adiabatic states with the angle are shown for different distances, chosen to lie approximately along the reaction minimum energy path.

The other two adiabatic states, $2\,^3A''$ and $1\,^3A'$, are linear at the transition state region as well as in most of the surfaces, as explained by the Σ^--Π vibronic effect, and do not show wells. As a result, the corresponding photodetachment spectra, in Fig. 9(b), do not show narrow resonances in contrast with the $1\,^3A''$ state, in Fig. 9(a). As discussed in Ref. 21, the different bands of the individual spectra are due to different HF vibrational levels. The spectrum for $1\,^3A''$ thus looks like that for $^3\Sigma^-$ in the collinear model, while those for $2\,^3A''$ and $1\,^3A'$ are connected to that of $^3\Pi$, in Fig. 5. The major differences arise at electron kinetic energy below 0.5 eV, and will be discussed below.

The initial wave packet is placed on top of the saddle point, as shown in Fig. 4. As a consequence, the oscillator strength of $1\,^3A''$ and $1\,^3A'$ corresponds to that of the $^3\Pi$,

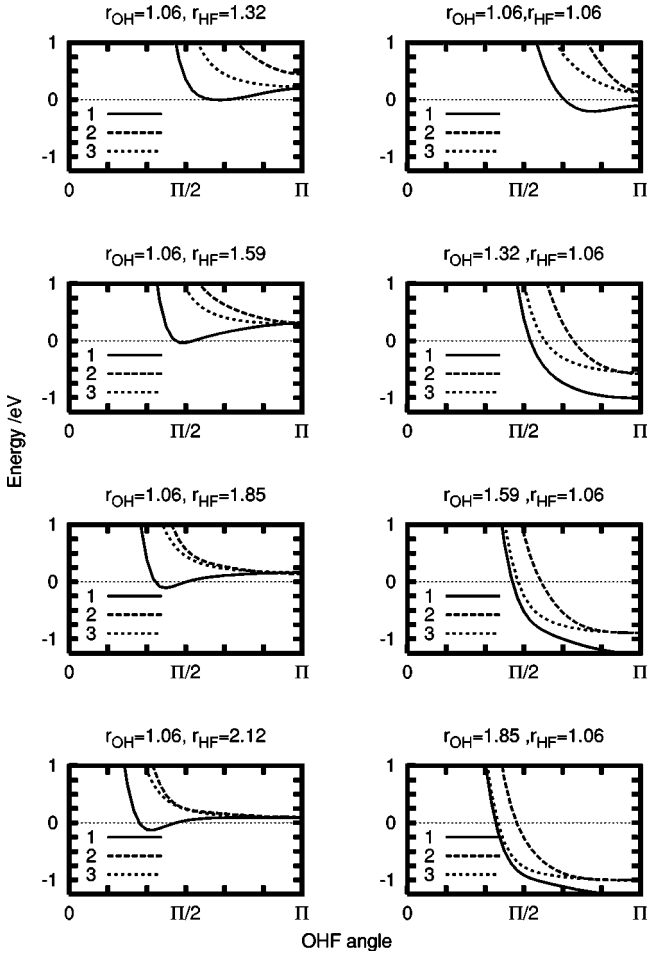

FIG. 10. Potential energy cuts as a function of the OHF angle for several distances along the minimum energy path of the triplet states of OHF: 1 is $1\,^3A''$, 2 is $2\,^3A''$, and 3 is $1\,^3A'$. The two conical intersections occur at $r_{OH}\approx 1$, $r_{HF}\approx 1.59$ Å, and at $r_{OH}\approx 1.05$, $r_{HF}\approx 1.2$ Å, before and after the saddle point, respectively.

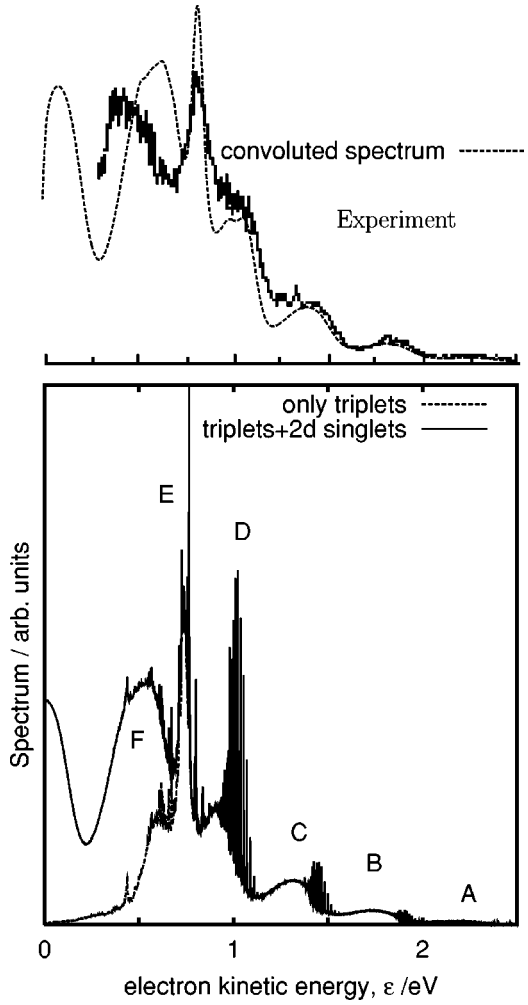

FIG. 11. Calculated photodetachment spectra obtained after averaging over all final triplet electronic states, using three-dimensional PESs and according to the transition matrix elements and multiplicity, as explained in the text. The experimental spectrum of Bradforth *et al.* (Ref. 22) is also shown for comparison in the top panel. The convoluted spectrum, thinner line of top panel, is obtained with a Gaussian, e^{-E^2/Γ^2}, $\Gamma=22$ meV.

while that of $2\,^3A''$ coincides with that of the $^3\Sigma^-$. Using the dipole moments of Table I and according to Eq. (4), the total spectrum obtained only for the three-dimensional triplets is shown in the bottom panel of Fig. 11. In order to better compare with the experimental result of Bradforth *et al.*,[22] the contributions from the two-dimensional singlets, shown in the preceding section, are included. The agreement with the experimental data of Bradforth *et al.*[22] is excellent, showing nearly the same sequence of peaks.

At this point, it should be noted that the narrow resonances do not appear in the experiment. This is expected because of the lower energy resolution and rotational average washes out such narrow structures. To simulate such effect, the total spectrum, in the bottom panel of Fig. 11, is convoluted with a Gaussian function. The result is shown in the top panel of Fig. 11 together with the experimental spectrum. The agreement in the sequence of bands, in position and intensity, is pretty good up to peak E. The position of peak F is not properly described because it corresponds to a two-dimensional simulation: if the angular zero-point energy is included, the spectrum will shift to higher OHF energy, and thus to lower electron kinetic energy. To improve the description of that peak, three-dimensional simulations on the singlet states are required.

To conclude this section, it should be stressed out that in the present simulation there is only one parameter that has been adjusted: since the dissociation energy of OHF^- is not known, the relation between the electron kinetic energy ϵ and the total energy of the neutral OHF system, E, has been fitted as (in eV) $\epsilon = h\nu + E_{OHF^-} - E = 0.95 - E$.

VI. NONADIABATIC DYNAMICS AT CONICAL INTERSECTIONS

Up to here, the overall features of the experimental spectrum are pretty well assigned. The total absorption spectrum is however a rather averaged quantity, so that it becomes rather insensitive to some peculiarities of the dynamics. In particular, the role of resonances is not clear in the experiment, and higher resolution would be desired to observe them.

Another important aspect is to what extent the reaction dynamics is adiabatic or not. It has been shown that there are

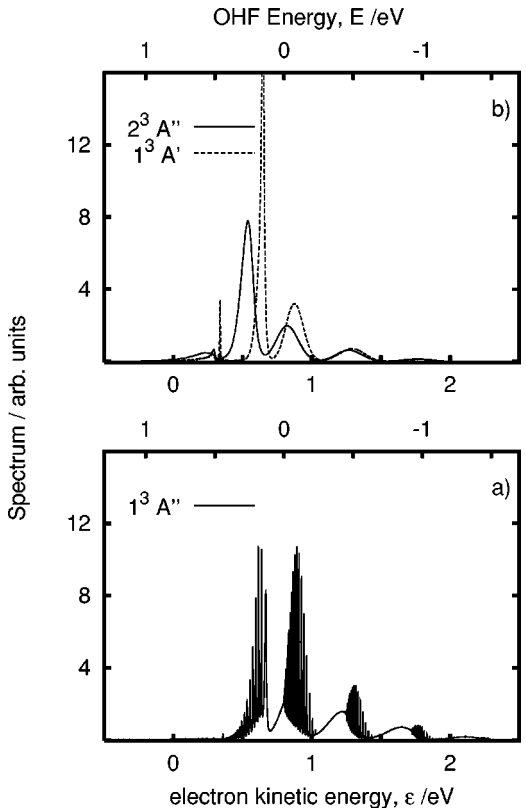

FIG. 12. Calculated photodetachment spectra for triplet electronic states of OHF using the fitted adiabatic surfaces but at collinear OHF configuration as a function of the electron kinetic energy (lower scale) and the internal OHF energy (upper scale) for (a) $1\ ^3A''$ and (b) $1\ ^3A'$ and $2\ ^3A''$ states.

several crossings between the $^3\Sigma^-$ and the $^3\Pi$ states at collinear configurations, giving rise to the ground adiabatic surface. In this situation, it is well known that vibronic effects are going to play an important role in the spectrum and dynamics.

In order to get an idea of such effects, in Fig. 12 the spectra obtained by doing two-dimensional wave backet calculations on the adiabatic surfaces at collinear geometry are shown. These spectra, on the adiabatic two-dimensional surfaces, are compared with those of Fig. 5, which can be considered to be on the diabatic two-dimensional representation. Since both of them correspond to collinear geometry, these states belong to different irreducible representations and there is no coupling between them. The spectrum of the adiabatic $1\ ^3A'$ is in nearly perfect agreement with that of the diabatic $^3\Pi$. The major differences arise for the adiabatic $^3A''$ states, which correspond to a mixture between the two diabatic surfaces. As a consequence, the spectra obtained for these states also correspond to a mixture. When the two spectra are added to get the total spectrum, the agreement is rather good, thus explaining why the agreement obtained with the adiabatic three-dimensional PESs is so good. However, for electron kinetic energies between 0 and 0.5 eV, the resonances in the two representations, diabatic and adiabatic, appear clearly at very different positions.

When the system bends the diabatic surfaces are coupled. It is expected that when considering a three-dimensional model of diabatic coupled states the spectrum will become closer to that obtained in the adiabatic picture. However, it is important to determine to what extent the dynamics is going to be diabatic or adiabatic. In particular, the HLH resonances described in the $1\ ^3A''$ are due to the presence of the wells and explore the transition state region. Since, the wells ''belong'' to the diabatic state correlating with $^3\Sigma^-$ state, while the lower barrier appears in the $^3\Pi$ diabatic states, these HLH resonances are expected to be very sensitive to the vibronic couplings in the vicinity of the conical intersections of this kind. A three-dimensional model of coupled diabatic states is now in progress to study such kind of Σ^--Π vibronic effects.

Moreover, the singlet states also show some crossings, specially in the entrance channel. Those states should also be modelized in a three-dimensional scheme of coupled diabatic states, in a case where there are six states correlating with $^1\Delta$, $^1\Pi$, $^1\Sigma^+$, and $^1\Sigma^-$ at collinear geometries. The influence of those states in the photodetachment spectrum only affects low electron kinetic energies. However, their interest lies in the reactive collisions and in the photodissociation from the deep well of the $^1A'$ state at bent geometries, as has been studied for related systems like OHCl near the dissociation threshold using overtone-overtone double resonance spectroscopy.[34–36]

VII. CONCLUSIONS

This work is devoted to a complete theoretical simulation of the photodetachment spectrum from the OHF^- anion towards several electronic states of the neutral OHF fragments. No *ad hoc* parameters has been used, except the dissociation energy of the anion. The $^2\Pi$ electronic states of the precursor anion are considered to be degenerate and uncoupled: the inclusion of Renner-Teller effects describing the splitting of the $^2\Pi$ states at bent geometries is left for a forthcoming paper.

Several electronic states of the neutral OHF system have been considered. In the first stage, the electronic states are calculated at collinear geometry including: $^3\Sigma^-$, $^3\Pi$, $^1\Delta$, $^1\Pi$, $^1\Sigma^+$, and $^1\Sigma^-$. The transition dipole moments have been approximated using a method in which the *ab initio* wave functions are included. Using a wave packet method, the photodetachment spectrum is simulated getting a rather good agreement with the experimental data of Bradforth *et al.*[22] The major disagreement concerns the relative intensity of the different bands, but the number and position of bands are clearly reproduced.

Since for electron kinetic energies above 0.5 eV only the triplet states contribute to the total photodetachment spectrum, three-dimensional calculations of the spectra on the three adiabatic triplet states were performed using the PESs recently proposed.[17,18] The simulated spectrum improves, becoming in excellent agreement with the experimental one.

At collinear geometry the $^3\Pi$ state crosses twice the $^3\Sigma^-$ one, which clearly asks for the necessity of building a three-dimensional diabatic potential model with, at least, three coupled triplet states to properly account for the reaction dynamics in the vicinity of these conical intersections. It has been shown that the resonances, appearing above the OH+F threshold on the $1\ ^3A''$ state, correspond to the light

H atom oscillating between the two wells, and passing over the transition state region. Since this region is the result of the vibronic interaction occurring specially in the vicinity of the conical intersection seams, those resonances should be delocalized among different diabatic states.

In particular, it has been found recently[18] that those HLH resonances mediate the reaction in the $OH(^2\Pi)+F(^2P) \rightarrow HF(^1\Sigma^+)+O(^3P)$ collision at energies below 0.15 eV, for the lower adiabatic surface. It is therefore expected that the nonadiabatic dynamics near the conical intersections described in this work is going to be important. Moreover, the reaction cross sections for the $2\,^3A''$ and $1\,^3A'$ adiabatic states show the presence of a threshold of about 0.3 eV. It is therefore important to determine if nonadiabatic couplings may contribute to significant electronic transitions which could give a reaction probability at lower energies. For that purpose a three-dimensional model of coupled diabatic states is required, and is now in construction.

Photodetachment spectra have been calculated for the first four singlets, too. They may contribute to the region of lower kinetic energy of the electron, peak F in the measured spectrum.[22] On the other hand, these states also present several crossings which may also produce interesting conical intersections as well. These states correlate with the higher $HF+O(^1D)$ asymptote, but, at the wavelength of 213 nm, this channel is only open with negligible kinetic energy of the electron. If the absorption to these states could be confirmed it might be interesting to increase the photon energy to have better access to them. In fact, these states could be directly accessed by direct photodissociation experiments from the deep well in a bent configuration in the ground $^1A'$ electronic state.

ACKNOWLEDGMENT

This work was supported by Ministerio de Ciencia y Tecnología (Spain) under Grant Nos. BFM2001-2179, BQU2001-0152, and BQU2002-04462-C02-01.

[1] R. P. Wayne, *Chemistry of Atmospheres*, 2nd ed. (Clarendon, Oxford, 2000).
[2] A. R. Ravishankara, G. Smith, R. T. Watson, and D. D. Davis, J. Phys. Chem. **81**, 2220 (1977).
[3] R. G. Macdonald and C. B. Moore, J. Chem. Phys. **68**, 513 (1978).
[4] D. J. Rakestraw, K. G. MaKendrick, and R. N. Zare, J. Chem. Phys. **87**, 7341 (1987).
[5] K. Mahmud, J.-S. Kim, and A. Fontijn, J. Phys. Chem. **94**, 2994 (1990).
[6] R. Zhang, W. J. van der Zande, M. J. Bronikowski, and R. N. Zare, J. Chem. Phys. **94**, 2704 (1991).
[7] M. J. Davis, H. Koizumi, G. C. Schatz, S. E. Bradforth, and D. M. Neumark, J. Chem. Phys. **101**, 4708 (1994).
[8] H. Koizumi, G. C. Schatz, and M. S. Gordon, J. Chem. Phys. **95**, 6421 (1991).
[9] N. Rougeau and C. Kubach, Chem. Phys. Lett. **274**, 535 (1997).
[10] B. Ramachandran, E. A. Schrader III, J. Senekowitsch, and R. E. Wyatt, J. Chem. Phys. **111**, 3862 (1999).
[11] L. Wang, C. Kalyanaraman, and A. B. McCoy, J. Chem. Phys. **110**, 11221 (1999).
[12] F. J. Aoiz, L. Bañares, J. F. Castillo, M. Menéndez, and J. E. Verdasco, Phys. Chem. Chem. Phys. **1**, 1149 (1999).
[13] K. Nobusada, H. Nakamura, Y. Lin, and B. Ramachandran, J. Chem. Phys. **113**, 1018 (2000).
[14] T. Xie, D. Wang, J. M. Bowman, and D. E. Manolopoulos, J. Chem. Phys. **116**, 7461 (2002).
[15] T. Xie, J. M. Bowman, K. A. Peterson, and B. Ramachandran, J. Chem. Phys. **119**, 9601 (2003).
[16] B. Ramachandran and K. A. Peterson, J. Chem. Phys. **119**, 9590 (2003).
[17] S. Gómez-Carrasco, L. González-Sánchez, A. Aguado, M. Paniagua, O. Roncero, M. L. Hernández, and J. M. Alvariño, Chem. Phys. Lett. **383**, 25 (2004).
[18] S. Gómez-Carrasco, L. González-Sánchez, A. Aguado, O. Roncero, J. M. Alvariño, M. L. Hernández, and M. Paniagua, J. Chem. Phys. **121**, 4605 (2004).
[19] J. J. Sloan, D. G. Watson, J. M. Williamson, and S. Wright, J. Chem. Phys. **75**, 1190 (1981).
[20] C. D. Walter and H. G. Wagner, Ber. Bunsenges. Phys. Chem. **87**, 403 (1983).
[21] L. González-Sánchez, S. Gómez-Carrasco, A. Aguado, M. Paniagua, M. L. Hernández, J. M. Alvariño, and O. Roncero, J. Chem. Phys. **121**, 309 (2004).
[22] S. E. Bradforth, D. W. Arnold, R. B. Metz, A. Weaver, and D. M. Neumark, J. Phys. Chem. **95**, 8066 (1991).
[23] R. N. Dixon and H. Tachikawa, Mol. Phys. **97**, 195 (1999).
[24] G. C. Schatz, J. Phys. Chem. **94**, 6157 (1990).
[25] R. B. Metz, S. E. Bradforth, and D. M. Neumark, Adv. Chem. Phys. **81**, 1 (1992).
[26] D. M. Neumark, Annu. Rev. Phys. Chem. **43**, 153 (1992).
[27] M. Paniagua, A. Aguado, M. Lara, and O. Roncero, J. Chem. Phys. **111**, 6712 (1999).
[28] A. Aguado, M. Paniagua, C. Sanz, and O. Roncero, J. Chem. Phys. **119**, 10088 (2003).
[29] MOLPRO is a package of *ab initio* programs designed by H.-J. Werner and P. J. Knowles, with contributions from J. Almlöf, R. D. Amos, A. Berning, M. J. O. Deegan, F. Eckert, S. T. Elbert, C. Hampel, R. Lindh W. Meyer, A. Nicklass, K. Peterson, R. Pitzer, A. J. Stone, P. R. Taylor, M. E. Mura, P. Pulay, M. Schütz, H. Stoll, T. Thorsteinsson, and D. L. Cooper (version 2002.7).
[30] F. L. Pilar, *Elementary Quantum Chemistry* (McGraw-Hill, New York, 1968).
[31] W. H. Press, S. A. Teukolsky, W. T. Vetterling, and B. P. Flannery, *Numerical Recipes* (Cambridge University Press, Cambridge, 1994).
[32] H. Tal-Ezer and R. Kosloff, J. Chem. Phys. **81**, 3967 (1984).
[33] C. Leforestier, R. H. Bisseling, C. Cerjan *et al.*, J. Comput. Phys. **94**, 59 (1991).
[34] A. Callegari, J. Rebstein, R. Jost, and T. R. Rizzo, J. Chem. Phys. **111**, 7359 (1999).
[35] A. Callegari, R. Schmied, P. Theulé, J. Rebstein, and T. R. Rizzo, Phys. Chem. Chem. Phys. **3**, 2245 (2001).
[36] G. Dutton, R. J. Barnes, and A. Sinha, J. Chem. Phys. **111**, 4976 (1999).
[37] S. Gómez-Carrasco, L. González-Sánchez, A. Aguado, O. Roncero, M. L. Hernández, J. M. Alvariño, and M. Paniagua (unpublished).
[38] H. Köppel, W. Domcke, and L. S. Cederbaum, Adv. Chem. Phys. **57**, 59 (1984).